AGU ADVANCING EARTH AND SPACE SCIENCES

Geophysical Research Letters

RESEARCH LETTER
10.1029/2024GL111857

Multi-Scale Thermal Mapping of Submarine Groundwater Discharge in Coastal Ecosystems of a Volcanic Area

Ebony L. Williams[1], Christopher B. Kratt[2], Raymond S. Rodolfo[3,4], Mark R. Lapus[4], Ryan R. Lardizabal[5], Aya S. Bangun[1], Amber T. Nguyen[1], Scott W. Tyler[2], and M. Bayani Cardenas[1]

[1]Department of Earth and Planetary Sciences, Jackson School of Geosciences, The University of Texas at Austin, Austin, TX, USA, [2]Department of Geological Sciences and Engineering, University of Nevada, Reno, NV, USA, [3]Department of Environmental Science, Ateneo de Manila University, Quezon City, Philippines, [4]Agricultural Sustainability Initiatives for Nature, Inc., Quezon City, Philippines, [5]Philsurv Geodetic Services, Mandaluyong City Metro Manila, Philippines

Abstract Submarine groundwater discharge (SGD) in volcanic areas commonly exhibits high temperatures, concentrations of metals and CO_2, and acidity, all of which could affect sensitive coastal ecosystems. Identifying and quantifying volcanic SGD is crucial yet challenging because the SGD might be both discrete, through fractured volcanic rock, and diffuse. At a volcanic area in the Philippines, the novel combination of satellite and drone-based thermal infrared remote sensing, ground-based fiber-optic distributed temperature sensing, and in situ thermal profiling in coastal sediment identified the multi-scale nature of SGD and quantified fluxes. We identified SGD across ∼30 km of coastline. The different approaches revealed numerous SGD signals from the intertidal zone to about a hundred meters offshore. In active seepage areas, temperatures peaked at 80°C, and Darcy fluxes were as high as 150 cm/d. SGD is therefore locally prominent and regionally important across the study area.

Plain Language Summary Submarine groundwater discharge (SGD) is the flow of groundwater from land to sea. SGD in volcanic areas can have high temperatures, high concentrations of heavy metals, high CO_2, and can be acidic, all of which impact sensitive coastal ecosystems. Quantifying volcanic SGD is important yet challenging because the flow can be diffuse and broadly distributed. At a volcanic area in the Philippines, the unique combination of satellite and drone-based thermal infrared remote sensing, ground-based fiber-optic distributed temperature sensing, and in situ thermal profiling in coastal sediment identified the multi-scale nature of SGD and quantified flow rates. We identified SGD across ∼30 km of coastline. The different approaches revealed numerous SGD signals from the intertidal zone (the region between high and low tide) to about a hundred meters offshore. At some locations, active seepage areas reached temperatures up to 80°C, and we calculated groundwater flow rates to be as high as 150 cm/day. SGD is therefore locally prominent and regionally important across the study area.

Key Points:

- Multi-scale thermal submarine groundwater discharge (SGD) was mapped in a volcanic area with coral reefs and marine protected areas
- Thermal SGD was prevalent in the area with both broadly diffuse signals and pronounced discrete discharge
- Local SGD reached 150 cm/d and 80°C

Supporting Information:

Supporting Information may be found in the online version of this article.

Correspondence to:

E. L. Williams,
ebony.williams@utexas.edu

Citation:

Williams, E. L., Kratt, C. B., Rodolfo, R. S., Lapus, M. R., Lardizabal, R. R., Bangun, A. S., et al. (2024). Multi-scale thermal mapping of submarine groundwater discharge in coastal ecosystems of a volcanic area. *Geophysical Research Letters*, *51*, e2024GL111857. https://doi.org/10.1029/2024GL111857

Received 7 AUG 2024
Accepted 12 OCT 2024

Author Contributions:

Conceptualization: Christopher B. Kratt, M. Bayani Cardenas
Data curation: Ebony L. Williams, Ryan R. Lardizabal
Formal analysis: Ebony L. Williams, M. Bayani Cardenas
Investigation: Ebony L. Williams, Christopher B. Kratt, Raymond S. Rodolfo, Mark R. Lapus, Ryan R. Lardizabal, Aya S. Bangun, Amber T. Nguyen, M. Bayani Cardenas
Methodology: Ebony L. Williams, Christopher B. Kratt, Raymond S. Rodolfo, Ryan R. Lardizabal, Scott W. Tyler, M. Bayani Cardenas
Project administration: M. Bayani Cardenas

1. Introduction

Submarine groundwater discharge (SGD), which is the flow of terrestrial fresh groundwater and recirculated seawater from continental and insular margin coastal aquifers to the ocean (Burnett et al., 2003; Moore, 1999; Taniguchi et al., 2019), is an important part of coastal environments because it brings solutes to the ocean at rates similar to rivers (Santos et al., 2021). This is the case despite SGD constituting <1% of fresh water that reaches coastlines globally (Luijendijk et al., 2020; Zhou et al., 2019). SGD is unequally distributed, with global analyses indicating that equatorial latitudes have higher SGD rates (Luijendijk et al., 2020; Zhou et al., 2019), and thus its importance is likewise expected to vary.

An important region within equatorial latitudes in the western Pacific is the Coral Triangle. This region is scientifically, ecologically, and economically important because it is home to over 76% of the worlds shallow-water, reef-building coral species (Veron et al., 2009). Not only is the region the epicenter of marine biodiversity, it is also volcanically active which creates geothermal environments that lead to hydrothermal SGD. Hydrothermal SGD (which we also refer to as thermal or volcanic SGD here) can have elevated groundwater discharge rates and exhibit high concentrations of dissolved metals, high CO_2, and low pH (Cardenas et al., 2020; Correa et al., 2021). All these can affect marine ecosystems profoundly. Under natural conditions, the thermal SGD provides important environmental context for coral reefs specifically because coral reef communities are

Resources: Raymond S. Rodolfo, Mark R. Lapus, Ryan R. Lardizabal, Scott W. Tyler, M. Bayani Cardenas
Supervision: Christopher B. Kratt, Raymond S. Rodolfo, Mark R. Lapus, Ryan R. Lardizabal, M. Bayani Cardenas
Visualization: Raymond S. Rodolfo, Mark R. Lapus
Writing – original draft: Ebony L. Williams
Writing – review & editing: Christopher B. Kratt, Scott W. Tyler, M. Bayani Cardenas

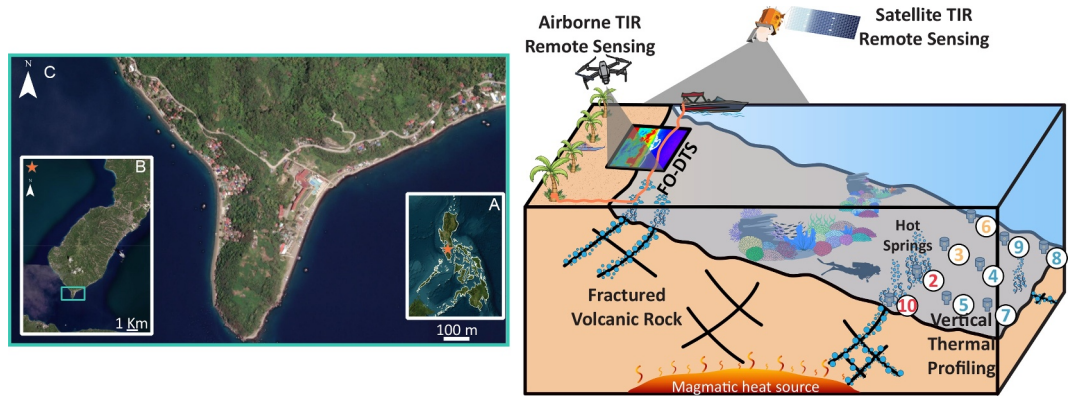

Figure 1. Left: location of the study area in the Philippines (a), with (b) displaying the Calumpan Peninsula, our regional focus area, and (c) displaying the southernmost tip of the Calumpan Peninsula, our local focus area. Right: a schematic of the four thermal sensing techniques employed in this study.

sensitive to acidification (Fabricius et al., 2011; Inoue et al., 2013). Volcanic SGD is also important for benthic ecosystems which have adapted to or whose community structure is shaped by this unique type of SGD (Hall-Spencer et al., 2008). Additionally, SGD is generally an important potential pathway for polluted groundwater to reach the ocean (Santos et al., 2021). Due to these reasons and the potential for prevalent thermal SGD throughout the Coral Triangle's vast coastline, it is important to detect, map, and quantify rates of volcanic SGD.

Quantifying and mapping SGD across broad regions is inherently challenging because of the many ways and scales over which SGD happens (Bratton, 2010; Santos et al., 2012). Hydrothermal processes further complicate the multi-scale dynamics of groundwater flow (Cardenas et al., 2012). However, thermal SGD offers advantages for mapping and measurement methods that use thermal signals. In this study, we pursue the idea that the novel combination of many thermal-based methods is key for developing a comprehensive view of SGD. We implemented this idea in Mabini, Batangas in the Philippines (Figure 1), a volcanically active region that lies within the Coral Triangle. Mabini, a town which covers most of the geographic feature known as the Calumpan Peninsula, is roughly at the center of an area referred to as "the center of the center" of coastal fish biodiversity (Carpenter & Springer, 2005). Recent studies in the area revealed that volcanic SGD delivers CO_2 and acidic waters to coastal areas with thriving coral reefs, some of which are protected areas and support the local economy (Cardenas et al., 2020; Correa et al., 2021). The primary objectives of this study are to map and quantify hydrothermal SGD across a volcanic coastal ecosystem, and to assess the limitations and advantages of different methods. We achieved these objectives by employing different thermal sensing techniques, all of which use temperature as an indirect tracer for submarine groundwater flow and capture this flow across different spatial scales.

2. Materials and Methods

We take advantage of the volcanic hydrogeologic setting to indirectly measure groundwater flow using heat as a natural tracer. We employed four thermal sensing techniques (Figure 1), which importantly capture SGD at nested spatial scales. The rationale is that thermal SGD should manifest as thermal anomalies across all scales.

We first utilized satellite thermal remote sensing by acquiring publicly available and processed Landsat 8 thermal infrared (TIR) scenes, which have a spatial resolution of 30 m, to ascertain the detectability of SGD thermal signatures from space and their distribution across the region (Jou-Claus et al., 2021). Next, we employed unmanned aerial system (UAS) remote sensing to capture SGD thermal signatures from the air. This method provides a finer spatial resolution of tens of centimeters along the coast and near shore (Kelly et al., 2013; Lee et al., 2016; Tamborski et al., 2015). Despite using uncalibrated imagery, UAS allows us to resolve thermal signatures with high precision and to accurately determine the area and morphology of these anomalies. The third technique we utilized is fiber-optic distributed temperature sensing (FO-DTS) (Read et al., 2013; Selker et al., 2006), which measures temperature at equal spatial intervals along a fiber optic cable with a resolution of ~50 cm. This method was used to detect SGD thermal signatures in the subtidal zone. Even though our data set includes uncalibrated temperature values, DTS allowed us to capture thermal signatures with high accuracy. To our knowledge, this is the first application of DTS in this region of the world. The final technique we employed is

vertical thermal profiling in coastal sediment tens of meters offshore under several meters of water. These profiles were analyzed using an analytical solution to heat transport to estimate vertical groundwater fluxes (Anderson, 2005; Constantz, 2008; Kurylyk et al., 2017; Rau et al., 2014). The spatial resolution of this method is typically determined by the spacing between the sensors. In this case, the instrument incorporates a 10 cm sensor spacing. Additional details about the methods are available in the supplementary information.

3. Results

In the following sections, we present data and results from the four thermal sensing methods utilized in this study, beginning with TIR satellite remote sensing, the broadest spatial scale, and ending with vertical thermal profiling, the finest spatial scale.

3.1. Satellite Thermal Remote Sensing

We used an algorithm to select Landsat 8 thermal band scenes that were useful. The algorithm returned 30 images from different time instances that met the cloud threshold mask; however, only 6 images had complete coverage of the area of interest. From this, we selected the best 3 images for further analysis. Visual inspection of these three images with any given color scale stretch did not highlight any plumes. This is likely because of the subtleties in plume temperatures, mixing, and that plumes are below the spatial resolution of the thermal images. In order to detect thermal anomalies, we created temperature transects along the coast from the best three images (see Figure S5 in Supporting Information S1), with temperatures extracted along the Calumpan Peninsula at distances of 30, 60, and 90 m away from the coastline; these distances represent an increase of one pixel away from the shoreline in the Landsat 8 thermal images. The temperature transects revealed consistent and persistent thermal anomalies ranging from 0.5°C to 4°C across each transect and across three different time instances (i.e., each best image) (Figure 2). Temperatures show warming trends that are replicable across certain areas along the coast and across each time instance; warming trends keep occurring at the same locations consistently across each transect and each time instance. The data shows that SGD is prevalent across the entire Calumpan Peninsula, occurring alongshore and offshore.

3.2. Airborne Thermal Remote Sensing

The UAS collected 2,384 images in both the green band centered on 0.56 m wavelength and the 8–14 m thermal band; we stitched these images together into a total of 9 semi-continuous orthomosaics of the Calumpan Peninsula coastline (see Figure S9 in Supporting Information S1). From these sections, numerous SGD anomalies were evident in the intertidal and subtidal zones (Figure 3), showcasing a greater image detail than the satellite remote sensing counterpart. We identified a total of 48 thermal anomalies; these were a mix of seepage zones, hotspots, and plumes. We subjectively and manually delineated thermal anomalies by drawing polygons around regions displaying substantially elevated temperatures relative to the surrounding ocean. We delineated the extent of these signals first in the thermal images and then in the visible images for context, in order to exclude thermal anomalies that are a result of objects such as rocks or boats. We then calculated the areas of each anomaly once we verified the delineations. Average UAS remotely sensed thermal anomalies varied across the entire peninsula (all nine orthomosaics) ranging from 29.6°C to 41.3°C, and averaged to 34.4°C; the average background ocean temperature of the nine orthomosaic sections was 29.37°C. The spatial extent of thermal anomalies ranged from 0.25 m^2 to 155.4 m^2. We identified several SGD anomalies in the southeastern and southern portion of the peninsula (about 60% of total plumes visually identified), perhaps indicating more SGD activity. UAS temperature-distance graphs (Figure 3) corroborate visually identified thermal plumes.

3.3. Distributed Temperature Sensing

The FO-DTS instrument revealed thermal anomalies in the subtidal zone along two 800 m transects on opposing sides of the southernmost tip of the Calumpan Peninsula (Figure 4). The detected anomalies on the western side cluster along the northwestern portion of the fiber-optic cable near the Twin Rocks MPA, with temperatures above background ocean temperature (~29.37°C) ranging from 31°C to 32°C. We calculated the background ocean temperature by averaging the offshore temperature values from each orthomosaic of the UAS imagery. On the eastern side, the detected anomalies were spread along the fiber-optic cable with a smaller range of temperatures from 30.5°C to 30.9°C. These thermal anomalies range from 0.1°C to 1°C, resembling the anomalies

10.1029/2024GL111857

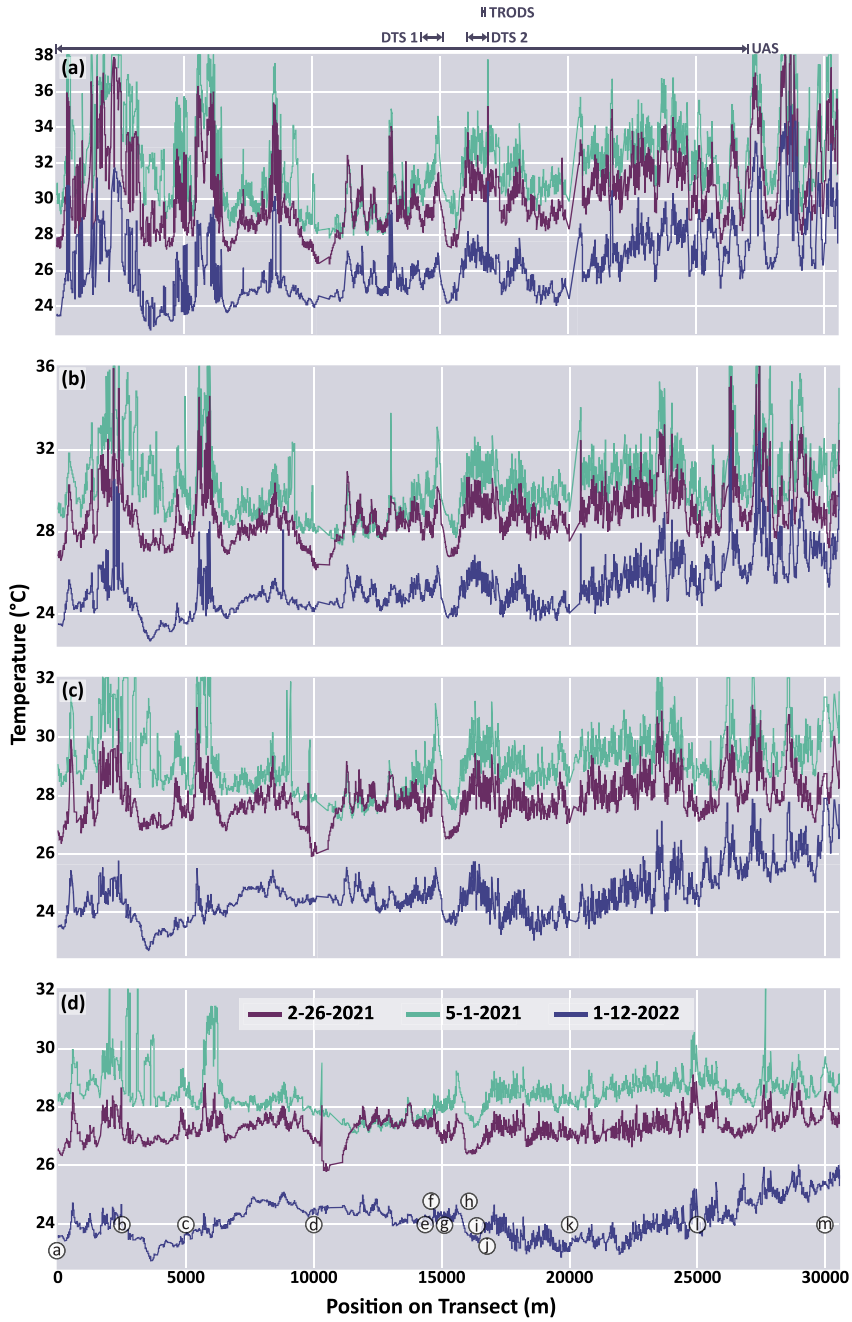

Figure 2. Satellite temperature transects surrounding the Calumpan Peninsula with distances of 0 (a; coastline), 30 (b), 60 (c), and 90 (d) meters away from the coastline. Each line contains extracted temperatures from the best three images (falling on February-26-2021, May-1-2021, and January-22-2022). The circled letters on panel (d) refer to points along the Calumpan Peninsula (see Figure S5 in Supporting Information S1). Above panel (a), the long arrow represents the extent of the unmanned aerial system surveys; the two shorter arrows represent the extents of the FO-DTS surveys, and the shortest arrow represents the extent of the thermal profiles (Trod survey). A normalized version of the satellite temperature traces, which visually enhances the comparison and highlights thermal anomalies, is included in the supplemental information (see Figure S7 in Supporting Information S1).

10.1029/2024GL111857

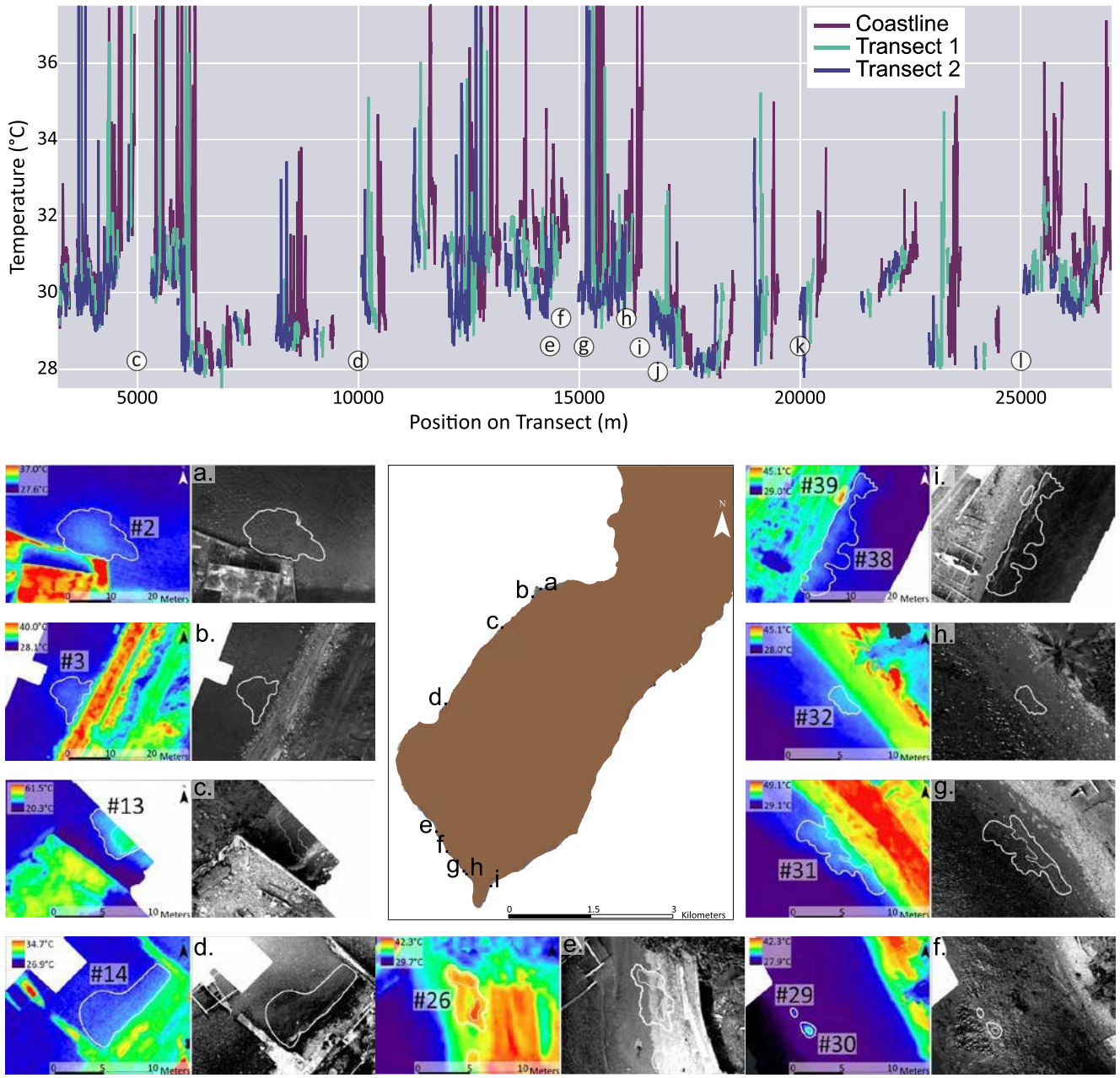

Figure 3. (Top) UAS temperature transects surrounding the Calumpan Peninsula with a distance of 0 m (Coastline), 5 m (Transect 1), and 10 m (Transect 2) from the coastline. All of these were captured during a single instance when the UAS was deployed in the field. (Bottom) Drone imagery displaying thermal band on the left and visual band 2 on the right. The white dashed lines delineate the extent of the plumes. Letters on the drone images correspond to those on the map indicating the image locations, and numbers correspond to the Submarine groundwater discharge identifier found in Table S3 in Supporting Information S1. A version of the drone temperature traces which are normalized and better compare and highlight thermal anomalies are included in the supplemental information (see Figure S10 in Supporting Information S1).

identified in the satellite and UAS imagery. Our field observations of thermal anomalies, which noted submarine springs and changing water temperatures along the fiber-optic cable, corroborate thermal anomalies identified with DTS measurements.

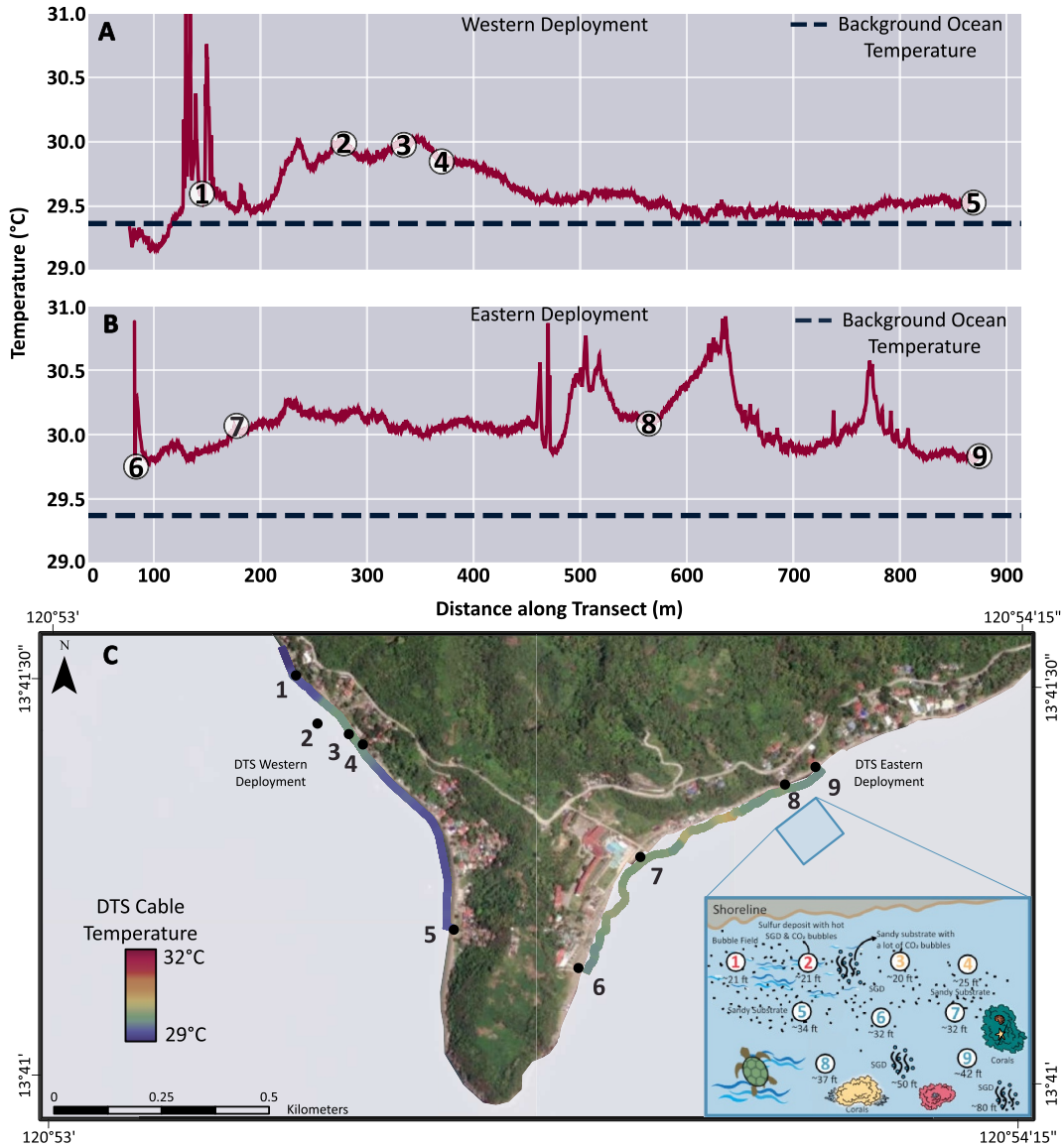

Figure 4. Temperature distance graphs (a, b) and schematic (c) for DTS transects around the tip of the Calumpan Peninsula. Panels (a, b) The background ocean temperature in (a, b) (29.37°C) were calculated by averaging the background ocean temperature values from all unmanned aerial system orthomosaics. Panel (c) DTS western deployment contains reference points 1 denoting a Rocky Bend in the coastline topography, 2 denoting the Twin Rocks MPA, 3 denoting a documented submarine spring, 4 denoting Planet Dive Resort which served as our base of operations, and 5 denoting Buceo Anilao Beach and Dive Resort. Panel (c) DTS eastern deployment contains reference points 6 denoting the Layag Resort, 7 denoting the Sea Spring Resort, 8 denoting the Searendipity Resort, and 9 denoting an Orange Roofed House. The inset map in panel (c) depicts the locations of the Trods, which are color coded in terms of relative magnitude of flux (i.e., red = high, yellow = moderate, low = blue).

3.4. Vertical Thermal Profiling and Vertical Darcy Fluxes

Vertical temperature profiling with instruments called Trods showed increasing temperature with depth in four out of nine deployment locations, thus indicating upwards heat flux (Figure 5) over a 20-hr span. These four temperature profiles have larger temperature gradients compared to the other five profiles, especially Profile 2 which spans a range of 40°C–90°C. We applied an analytical solution to the one-dimensional heat advection-conduction equation to each of the profiles to estimate vertical Darcy fluxes; four of these fluxes indicate upward flow (from the same four profiles aforementioned), and the remaining five indicate weak downward flow. Average SGD Darcy

10.1029/2024GL111857

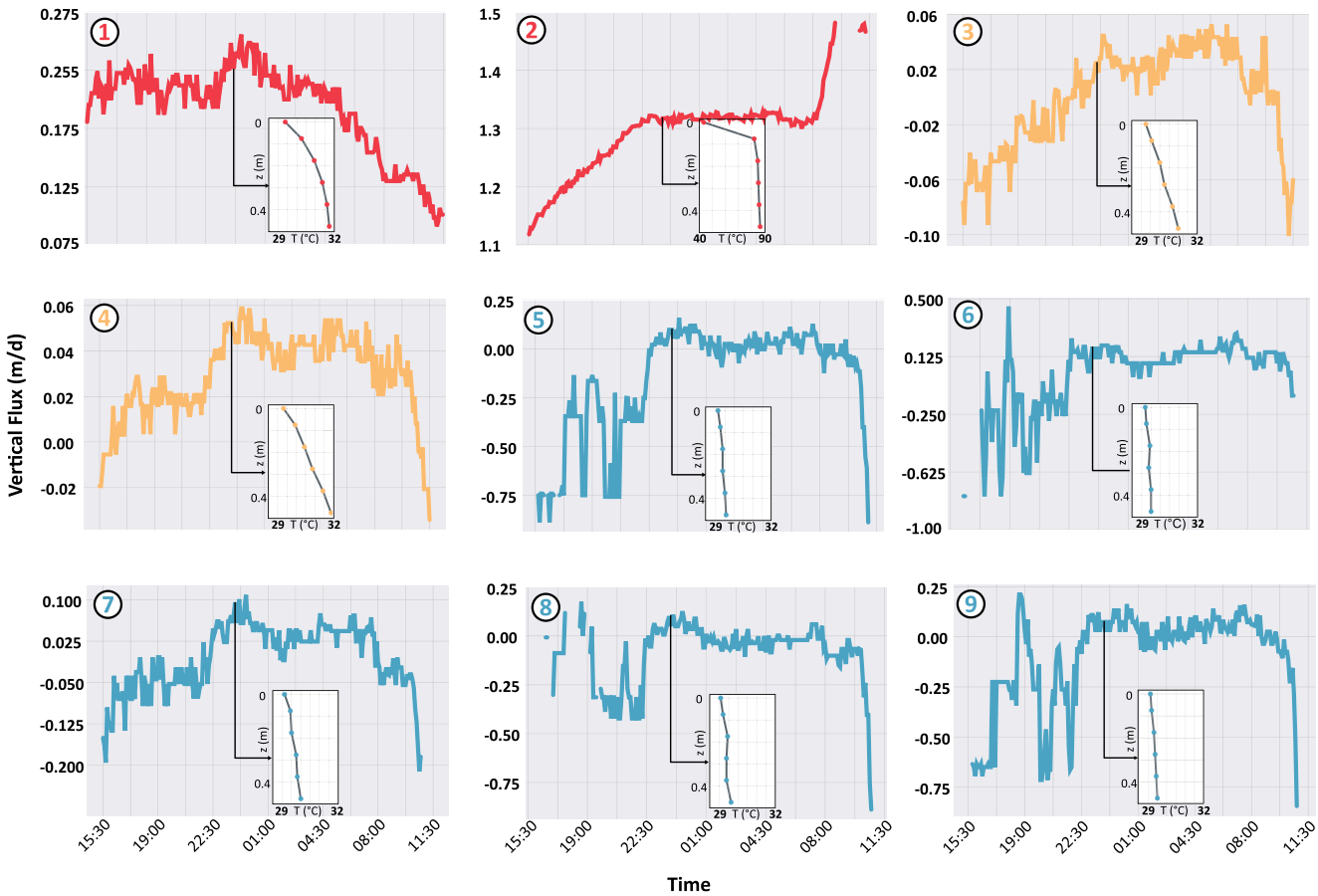

Figure 5. Vertical temperature fluxes with one corresponding temperature profile for the 9 Trods deployed. Fluxes are color coded by the relative magnitude of discharge: red = moderate to high discharge, yellow = low to moderate discharge, and blue = no to low discharge. The inset schematic in Figure 4 display the approximate locations of the Trods.

flux rates range from 1 cm/d to 25 cm/d, except for Profile 2 which has an average rate of 131 cm/d. Locations of the Trods reveal preferential SGD along the same northeast-southwest strike in an area offshore.

4. Discussion

4.1. Regional Scale SGD

We assessed SGD across the Calumpan Peninsula region through satellite and UAS remote sensing, with each technique covering over 25,000 m of coastline and depicting a broad view of thermal signals across the region. The satellite graphs highlight persistent thermal anomalies across the entire Calumpan Peninsula, suggesting fields of plumes that discharge consistently at a scale large enough for detection by the Landsat 8 TIRS sensor. These warm regions are present over all four transects; however, Transects 2 and 3 (Figure 2, panels c, d) provide a stronger argument for thermal anomalies being SGD, as they are 60 and 90 m offshore respectively, and are unaffected by overprinting land pixel temperatures. In the UAS imagery, we identify numerous plumes with varying sizes in greater clarity. We identify most plumes along the southern and southernwestern portions of the Calumpan Peninsula, spatially indicating "hot spots" of SGD activity in both the subtidal and intertidal zones.

In comparing the satellite and UAS remote sensing techniques, we see that the UAS detects similar temperatures to the satellite imagery, and detects plumes in the same location as the warm regions identified in the satellite imagery, and having similar temperature anomaly ranges. The UAS imagery captured about 31% of the satellite imagery coastline transect and confirmed 12 locations of suspected SGD identified in the satellite imagery. These 12 locations (highlighted in Table S3 in Supporting Information S1) either overlap directly with or are near the

satellite coastline transect. When assessing regional SGD, the UAS provides a more robust method as it can detect potentially prevalent small SGD plumes with a thermal pixel resolution of 160 × 120 pixels.

4.2. Local Scale SGD

Both UAS and DTS capture local scale SGD with thermal anomalies in the intertidal and subtidal zones at fine spatial and temporal resolution. The DTS temperature traces highlight thermal spatial variations. DTS deployment 1 thermal anomalies clustered toward the beginning of the cable, indicating a pronounced SGD zone. These anomalies happen to be near the Twin Rocks MPA where the literature documents a nearby spring (Cardenas et al., 2020; Correa et al., 2021). DTS deployment 2 anomalies were more distributed along the cable, that is, there are four "groupings" of anomalies that span the length of the cable. The DTS data suggests that the eastern side of the Mabini Peninsula experiences higher SGD activity compared to the western side, indicating more favorable pathways for SGD on the eastern side.

The location of the DTS cable overlapped with some areas covered by the UAS on opposing sides of the Mabini Peninsula. There were however, only two thermal anomalies detected from DTS that directly overlap with UAS identified plumes, one on the western side and one on the eastern side of the Mabini Peninsula. Both DTS thermal anomalies do not match either the minimum or average temperatures from the UAS identified plumes, as the DTS temperatures consistently register a few degrees lower than the UAS temperatures. This difference in anomaly temperature results from the data being uncalibrated for sensor drift. UAS and DTS thermal sensing techniques are powerful methods in capturing local SGD, but from opposite and complementary ends: UAS captures plumes as they reach the ocean's surface and DTS captures plumes originating from the seabed. DTS is sensitive to both narrow point source and spatially diffuse SGD, but the logistics of deployment pose difficulty in this coastal setting due to waves and highly variable coastlines with sandy, rock, and coral covered zones. UAS is a more convenient yet equally robust method in detecting SGD.

4.3. Point Scale SGD

Trods provided insights into how heat and water travel through the seabed over a 20-hr deployment period. Trods 1, 2, 3, and 4 all indicated advecting heat and upwelling submarine groundwater, especially Trod 2 which yielded the highest groundwater temperatures and fluxes. These Trods all lie in the same E-W horizontal strike, indicating a localized zone of offshore discharge. Trod 2 temperatures and fluxes are high, most likely due to an unnamed fault striking roughly 343° NE/SE directing the flow of hydrothermal waters. The remaining Trods show no to low SGD even though they were located only 10's of meters away from Trods 1, 2, 3, 4, and nearby a documented submarine spring; these two pieces of evidence allowed us to generally determine preferential and non-preferential outflow points, and even hint at flow patterns occurring offshore.

The location of each Trod lies within a single 30-m Landsat 8 thermal pixel; however, the discharging submarine groundwater does not reach the surface or discharge at a scale large enough for detection by the Landsat TIRS sensor. The Trods identified and quantified anomalies that did not appear in any of the three Landsat 8 images (see Figure S5 in Supporting Information S1). Nonetheless, Trods proved highly effective in measuring point thermal and fluid fluxes.

4.4. Caveats and Limitations

This work represented a vast effort to identify and quantify SGD across the study region in the Philippines, and was successful in doing so. Despite the new insights revealed, the results further justify the need for a comprehensive study of SGD in this region, particularly mechanistic studies that can explain the multi-scale observations. Furthermore, this work has caveats that require attention. A major caveat is that we only covered a narrow time period. We do not know if the estimated flow rates are high or low for this region based on the current data; to reveal this, Trod sensors need long term deployment in multiple locations, perhaps over different tidal cycles and seasons, to yield a more accurate and comprehensive view of SGD. Another important caveat is that the visual plume identification is subjective. Although we are confident in our delineations of plumes based on clear UAS imagery and regional context, some plumes were hard to determine and delineate due to UAS post processing stitching errors. Training algorithms with temperature thresholds can enhance the robustness of visual identification for delineating plumes. One last caveat to acknowledge is the inherent limitation with each thermal sensor utilized. The Landsat 8 thermal sensor provides coarse spatial resolution that is

unable to clearly delineate any SGD plume structure. On the other hand, UAS, although spatially and temporally finer in scale, cannot capture plumes or signals emerging from the seabed that do not reach the ocean's surface. DTS measures temperature by integrating over ∼25 cm of optical fiber, potentially smoothing temperature variability at scales less than the spatial resolution of the instrument (here ∼50 cm). DTS cable deployments can be logistically challenging and the cable may be subject to damage by wave action or marine crafts and fishing gear. Trods yield powerful information, but only within 0.5 m of the seabed, which may not be deep enough to capture full vertical variations of heat transport and flow. Because of these, we combined different methods.

5. Conclusions

This study utilized four thermal sensing techniques that encompass different spatial scales to map locations of SGD across the Calumpan Peninsula in the Philippines. The Landsat 8 TIRS sensor revealed several perpetually warm areas along the peninsula, suggesting thermal signals associated with SGD are prevalent and widespread throughout this region. UAS TIR sensor detected SGD hotspots and plumes across the intertidal and subtidal zones throughout regions spanning the Calumpan Peninsula. Hotspots and plumes ranged in temperatures from 29.57°C to 41.25°C, and ranged in areas from 0.25 m^2 to 155.4 m^2. DTS recorded thermal signals in the subtidal zone along the peninsula, with the largest recorded temperature of 32.1°C on the western side and 30.9°C on the eastern side. Vertical thermal profiling in the seabed 80 m offshore detected thermal signals which reached temperatures over 80°C, and estimated fluxes reaching as high as 150 cm/day. We find that UAS TIR remote sensing and vertical thermal profiling are the most feasible thermal sensing methods applicable to this region, as they measure SGD from different scales, and provide important quantitative information such as plume morphology and discharge rates. These findings provide insights into the spatial variations of SGD, which can later inform groundwater flow and transport modeling at both point and regional scales. This work can also be beneficial to local and regional ecosystem management organizations, as well as marine biologists and ecologists studying the impacts of SGD on coastal ecosystems.

Data Availability Statement

The thermal data used in this study and key results are available at Hydroshare (Williams, 2024) with a Creative Commons Attribution 4.0 International license. Satellite thermal remote sensing data are publicly available from USGS and can be easily accessed through Google Earth Engine (https://developers.google.com/earth-engine/datasets/catalog/LANDSAT_LC08_C02_T1_L2).

Acknowledgments
We thank the National Science Foundation (CTEMPS), under Grant EAR-1832170, the Geological Society of America Graduate Student Geoscience Grant (13665-22), and the Geology Foundation at The University of Texas at Austin for funding this work.

References

Anderson, M. P. (2005). Heat as a ground water tracer. *Ground Water*, *43*(6), 951–968. https://doi.org/10.1111/j.1745-6584.2005.00052.x

Bratton, J. F. (2010). The three scales of submarine groundwater flow and discharge across passive continental margins. *The Journal of Geology*, *118*(5), 565–575. https://doi.org/10.1086/655114

Burnett, W. C., Bokuniewicz, H., Huettel, M., Moore, W. S., & Taniguchi, M. (2003). Groundwater and pore water inputs to the coastal zone. *Biogeochemistry*, *66*(1/2), 3–33. https://doi.org/10.1023/b:biog.0000006066.21240.53

Cardenas, M. B., Lagmay, A. M. F., Andrews, B. J., Rodolfo, R. S., Cabria, H. B., Zamora, P. B., & Lapus, M. R. (2012). Terrestrial smokers: Thermal springs due to hydrothermal convection of groundwater connected to surface water. *Geophysical Research Letters*, *39*(2). https://doi.org/10.1029/2011gl050475

Cardenas, M. B., Rodolfo, R. S., Lapus, M. R., Cabria, H. B., Fullon, J., Gojunco, G. R., et al. (2020). Submarine groundwater and vent discharge in a volcanic area associated with coastal acidification. *Geophysical Research Letters*, *47*(1), e2019GL085730. https://doi.org/10.1029/2019GL085730

Carpenter, K. E., & Springer, V. G. (2005). The center of the center of marine shore fish biodiversity: The Philippine Islands. *Environmental Biology of Fishes*, *72*(4), 467–480. https://doi.org/10.1007/s10641-004-3154-4

Church, T. M. (1996). An underground route for the water cycle. *Nature*, *380*(6575), 579–580. https://doi.org/10.1038/380579a0

Constantz, J. (2008). Heat as a tracer to determine streambed water exchanges. *Water Resources Research*, *44*(4). https://doi.org/10.1029/2008WR006996

Correa, R. E., Cardenas, M. B., Rodolfo, R. S., Lapus, M. R., Davis, K. L., Giles, A. B., et al. (2021). Submarine groundwater discharge releases CO_2 to a coral reef. *ACS ES&T Water*, *1*(8), 1756–1764. https://doi.org/10.1021/acsestwater.1c00104

Fabricius, K. E., Langdon, C., Uthicke, S., Humphrey, C., Noonan, S., De'ath, G., et al. (2011). Losers and winners in coral reefs acclimatized to elevated carbon dioxide concentrations. *Nature Climate Change*, *1*(3), 165–169. https://doi.org/10.1038/nclimate1122

Hall-Spencer, J. M., Rodolfo-Metalpa, R., Martin, S., Ransome, E., Fine, M., Turner, S. M., et al. (2008). Volcanic carbon dioxide vents show ecosystem effects of ocean acidification. *Nature*, *454*(7200), 96–99. https://doi.org/10.1038/nature07051

Inoue, S., Kayanne, H., Yamamoto, S., & Kurihara, H. (2013). Spatial community shift from hard to soft corals in acidified water. *Nature Climate Change*, *3*(7), 683–687. https://doi.org/10.1038/nclimate1855

Jou-Claus, S., Folch, A., & Garcia-Orellana, J. (2021). Applicability of Landsat 8 thermal infrared sensor for identifying submarine groundwater discharge springs in the Mediterranean Sea basin. *Hydrology and Earth System Sciences*, *25*(9), 4789–4805. https://doi.org/10.5194/hess-25-4789-2021

Kelly, J. L., Glenn, C. R., & Lucey, P. G. (2013). High-resolution aerial infrared mapping of groundwater discharge to the coastal ocean. *Limnology and Oceanography: Methods*, *11*(5), 262–277. https://doi.org/10.4319/lom.2013.11.262

Kurylyk, B. L., Irvine, D. J., Carey, S. K., Briggs, M. A., Werkema, D. D., & Bonham, M. (2017). Heat as a groundwater tracer in shallow and deep heterogeneous media: Analytical solution, spreadsheet tool, and field applications. *Hydrological Processes*, *31*(14), 2648–2661. https://doi.org/10.1002/hyp.11216

Lee, E., Yoon, H., Hyun, S. P., Burnett, W. C., Koh, D.-C., Ha, K., et al. (2016). Unmanned aerial vehicles (UAVs)-based thermal infrared (TIR) mapping, a novel approach to assess groundwater discharge into the coastal zone. *Limnology and Oceanography: Methods*, *14*(11), 725–735. https://doi.org/10.1002/lom3.10132

Luijendijk, E., Gleeson, T., & Moosdorf, N. (2020). Fresh groundwater discharge insignificant for the world's oceans but important for coastal ecosystems. *Nature Communications*, *11*(1260), 1260. https://doi.org/10.1038/s41467-020-15064-8

Moore, W. S. (1999). The subterranean estuary: A reaction zone of ground water and sea water. *Marine Chemistry*, *65*(1), 111–125. https://doi.org/10.1016/S0304-4203(99)00014-6

Rau, G. C., Andersen, M. S., McCallum, A. M., Roshan, H., & Acworth, R. I. (2014). Heat as a tracer to quantify water flow in near-surface sediments. *Earth-Science Reviews*, *129*, 40–58. https://doi.org/10.1016/j.earscirev.2013.10.015

Read, T., Bour, O., Bense, V., Le Borgne, T., Goderniaux, P., Klepikova, M. V., et al. (2013). Characterizing groundwater flow and heat transport in fractured rock using fiber-optic distributed temperature sensing. *Geophysical Research Letters*, *40*(10), 2055–2059. https://doi.org/10.1002/grl.50397

Santos, I. R., Chen, X., Lecher, A. L., Sawyer, A. H., Moosdorf, N., Rodellas, V., et al. (2021). Submarine groundwater discharge impacts on coastal nutrient biogeochemistry. *Nature Reviews Earth & Environment*, *2*(5), 307–323. https://doi.org/10.1038/s43017-021-00152-0

Santos, I. R., Eyre, B. D., & Huettel, M. (2012). The driving forces of porewater and groundwater flow in permeable coastal sediments: A review. *Estuarine, Coastal and Shelf Science*, *98*, 1–15. https://doi.org/10.1016/j.ecss.2011.10.024

Selker, J., van de Giesen, N., Westhoff, M., Luxemburg, W., & Parlange, M. B. (2006). Fiber optics opens window on stream dynamics. *Geophysical Research Letters*, *33*(24). https://doi.org/10.1029/2006GL027979

Tamborski, J. J., Rogers, A. D., Bokuniewicz, H. J., Cochran, J. K., & Young, C. R. (2015). Identification and quantification of diffuse fresh submarine groundwater discharge via airborne thermal infrared remote sensing. *Remote Sensing of Environment*, *171*, 202–217. https://doi.org/10.1016/j.rse.2015.10.010

Taniguchi, M., Dulai, H., Burnett, K. M., Santos, I. R., Sugimoto, R., Stieglitz, T., et al. (2019). Submarine groundwater discharge: Updates on its measurement techniques, geophysical drivers, magnitudes, and effects. *Frontiers in Environmental Science*, *7*. https://doi.org/10.3389/fenvs.2019.00141

Veron, J. E. N., Devantier, L. M., Turak, E., Green, A. L., Kininmonth, S., Stafford-Smith, M., & Peterson, N. (2009). Delineating the coral Triangle. *Galaxea, Journal of Coral Reef Studies*, *11*(2), 91–100. https://doi.org/10.3755/galaxea.11.91

Williams, E. (2024). Multi-scale thermal mapping of submarine groundwater discharge in coastal ecosystems of a volcanic area [Dataset]. *HydroShare*. https://doi.org/10.4211/hs.b5bcc8ea9e2146e892a5390d9c083d15

Zhou, Y., Sawyer, A. H., David, C. H., & Famiglietti, J. S. (2019). Fresh submarine groundwater discharge to the near-global coast. *Geophysical Research Letters*, *46*(11), 5855–5863. https://doi.org/10.1029/2019GL082749

References From the Supporting Information

Abolt, C., Caldwell, T., Wolaver, B., & Pai, H. (2018). Unmanned aerial vehicle-based monitoring of groundwater inputs to surface waters using an economical thermal infrared camera. *Optical Engineering*, *57*(5), 053113. https://doi.org/10.1117/1.OE.57.5.053113

Bredehoeft, J. D., & Papadopulos, I. S. (1965). Rates of vertical groundwater movement estimated from the Earth's thermal profile. *Water Resources Research*, *1*(2), 325–328. https://doi.org/10.1029/WR001i002p00325

Demir, C. (2022). Auto-FLUX-LM. *GitHub*. Retrieved from https://github.com/cannsudemir/Auto-FLUX-LM

Shan, C., & Bodvarsson, G. (2004). An analytical solution for estimating percolation rate by fitting temperature profiles in the vadose zone. *Journal of Contaminant Hydrology*, *68*(1), 83–95. https://doi.org/10.1016/S0169-7722(03)00126-8

Tyler, S. W., Selker, J. S., Bogaard, T., van de Giesen, N., & Aquilar-Lopez, J. (2022). Distributed fiber-optic hydrogeophysics. The Groundwater Project. https://doi.org/10.21083/978-1-77470-031-0

Tyler, S. W., Selker, J. S., Hausner, M. B., Hatch, C. E., Torgersen, T., Thodal, C. E., & Schladow, S. G. (2009). Environmental temperature sensing using Raman spectra DTS fiber-optic methods. *Water Resources Research*, *45*(4). https://doi.org/10.1029/2008WR007052

USGS/EROS. (2020). LSDS-1328. Landsat 8-9 operational land imager (OLI) thermal infrared sensor (TIRS) collection 2 level 2 (L2) data format control book (DFCB).

Van de Giesen, N., Steele-Dunne, S. C., Jansen, J., Hoes, O., Hausner, M. B., Tyler, S., & Selker, J. (2012). Double-ended calibration of fiber-optic Raman spectra distributed temperature sensing data. *Sensors*, *12*(5), 5471–5485. Article 5. https://doi.org/10.3390/s120505471